RSC Advances

PAPER

View Article Online
View Journal | View Issue

Cite this: *RSC Adv.*, 2017, **7**, 39034

Toward improved mechanical strength, oxidative stability and proton conductivity of an aligned quadratic hybrid (SPEEK/FPAPB/Fe_3O_4-FGO) membrane for application in high temperature and low humidity fuel cells†

Mohanraj Vinothkannan,[a] Ae Rhan Kim,*[b] G. Gnana kumar,[c] Jeong-Mo Yoon[d] and Dong Jin Yoo*[ae]

Iron oxide (Fe_3O_4) anchored functionalized graphene oxide (FGO) is applied as a magnetically active filler as well as a solid proton conductor to realize an aligned hybrid membrane architecture with blended polymer matrix consisting of fluorinated poly arylene propane biphenyl (FPAPB) and sulfonated poly ether ether ketone (SPEEK) for application in high temperature and low humidity fuel cells. The simple, but effective, functionalization of GO is performed with sulfonic acid (SO_3H) containing organosilane to increase the per unit volume of SO_3H groups and is then anchored by Fe_3O_4 nanoparticles to create the magnetic property. A constant magnetic field of 0.25 T is applied to perpendicularly align Fe_3O_4-FGO to the cross-section surface of membrane during solution casting process. The carbon skeleton of aligned Fe_3O_4-FGO and C–F bonds of FPAPB allow for an unprecedented approach to tailor the mechanical strength and oxidative stability of quadratic hybrid membrane, as evidenced by the results of dynamic mechanical analysis (DMA) and *ex situ* durability test. The incorporation of aligned Fe_3O_4-FGO improves water absorption, ion exchange capacity and proton conductivity of membrane by increasing the number of SO_3H groups per unit volume of membrane domain, while retaining considerable dimensional stability. The peak proton conductivity of aligned SPFSGF-5 membrane at 120 °C under 20% RH is 11.13 mS cm^{-1}, which is 1.44 fold better than that of pristine SP membrane (7.68 mS cm^{-1}). In contrast, under identical operating conditions, the Nafion-112 membrane exhibited a peak proton conductivity of 9.78 mS cm^{-1}, a 1.13 fold lower conductivity compared to aligned quadratic hybrid membrane. Furthermore, the aligned quadratic hybrid membrane exhibited lower H_2 and O_2 gas permeability compared to pristine SP and unaligned quadratic hybrid membranes.

Received 26th June 2017
Accepted 24th July 2017

DOI: 10.1039/c7ra07063b

rsc.li/rsc-advances

1. Introduction

Polymer electrolyte fuel cell (PEFC) technology is an important part of the hydrogen economy.[1,2] PEFCs help to remedy issues such as energy insecurity due to the depletion of fossil fuels and also contribute to environmentally benign energy use, offering trivial/zero production of pollutant gases, high conversion efficiency to produce electricity from hydrogen and extraordinary energy density.[3–5] The proton exchange membrane (PEM) is a critical element that underpins the overall electrochemical performance of the PEFC,[6,7] and perfluorosulfonic acid (PFSA) membranes, such as Nafion, have been extensively studied as standard PEMs for PEFCs, due to their elevated chemical stability under a strong radical environment, high mechanical stability and high proton conductivity.[8,9] However, PFSA membranes are expensive due to their complex synthesis, exhibit poor fuel barrier properties, and their proton conductivity is susceptible to water drift in the membrane.[10,11] As a result, widespread interest on PFSA membranes has faded. Accordingly, researchers have attempted to develop modified PFSA membranes or to design alternative PEMs. A good PEM should be cost effective, offer excellent proton conductivity under low humidity or anhydrous condition and exhibit

[a]*Graduate School, Department of Energy Storage/Conversion Engineering, Hydrogen and Fuel Cell Research Center, Chonbuk National University, Jeollabuk-do 54896, Republic of Korea. E-mail: djyoo@jbnu.ac.kr*

[b]*R&D Center for CANUTECH, Business Incubation Center of Chonbuk National University, Jeollabuk-do 54896, Republic of Korea. E-mail: canutech@hanmail.net*

[c]*Department of Physical Chemistry, School of Chemistry, Madurai Kamaraj University, Madurai 625021, Tamil Nadu, India*

[d]*Division of New Materials Engineering, Chonbuk National University, Jeollabuk-do 54896, Republic of Korea*

[e]*Department of Life Science, Chonbuk National University, Jeollabuk-do 54896, Republic of Korea*

† Electronic supplementary information (ESI) available. See DOI: 10.1039/c7ra07063b

sustainable durability under diverse operating environments.[12] These would make a PEFC system efficient, cost effective, durable and reliable.

Aromatic hydrocarbon polymers, especially poly ether ether ketone (PEEK), are notable for their attributes including low cost, easy sulfonation and processability, high thermal and mechanical stabilities and excellent film forming tendency.[13,14] Thus, exploitation of PEEK for PEM applications is being thrived. Proton conductivity of the PEM can be increased with the degree of sulfonation (DS) of sulfonated PEEK (SPEEK), but it reduces thermal stability and mechanical strength.[15] At high DS level, the hydrophilic SO_3H channels generate incompatibility with hydrophobic polymer chains, which lead to generation of tears and pinholes on the surface of PEM during solution casting.[14] In addition, chemical degradation of the polymer chains, caused by hydroxyl ($HO^{\bullet}$) and hydroperoxyl ($HOO^{\bullet}$) radicals in the cathode side during PEFC operation, can aggravate the tears and pinholes on PEM.[16] Altogether, these issues result in cyclical swelling and shrinking of SPEEK membrane (high DS), and consequently lead to high perviousness of hydrogen and mixed potential with oxygen. These may adversely minimize the PEFC efficiency by inefficient fuel usage and reducing the cell voltage.

Blending an optimal amount of hydrophobic polymer is the most favourable approach to improve mechanical strength, oxidative stability and fuel barrier properties of PEM while retaining reasonable proton conductivity.[14,17] Fluorinated polymers have shown good tensile stiffness, aqueous, acid and radical resistance, considerable viscosity and pore filling characteristics. Also, the backbone chains of fluorinated polymers enable the PEM to retain high compatibility with fluorinated binders, such as PTFE and Nafion, assisting in the construction of highly durable MEA with low cell resistance.[18–20] Inspired by such unique properties, fluorinated polymers are being extensively studied in PEM reinforcement processes.

Meanwhile, huge scientific and industrial attention is focused on high temperature PEFCs, due to their swift electrode reaction kinetics, minimization of expensive auxiliary units (external humidifier) and negligible electro-catalyst poisoning.[21,22] One of the best ways to the real-time applications of such PEFC is to exploit a PEM that capable to operate at high temperature and low humidity conditions. Unfortunately, the water swollen SPEEK membrane is adversely dehumidified when exposed to this stringent condition. To this end, the membrane needs to be suitably composed with hygroscopic fillers, such as TiO_2, Fe_2O_3, SiO_2, ZrO_2 and zeolite nanostructures, which have been extensively studied over the past decade for use in PEM of high temperature PEFCs.[23–27]

Graphene (sp^2 hybridized 2-dimensional sheets) belongs to a fascinating class of carbon nanomaterials, it was discovered by Geim *et al.* in 2004.[28] It is associated with extended specific surface (2630 $m^2\ g^{-1}$), thin backbone skeleton, intrinsic tensile strength (130 GPa), high Young's modulus (1 TPa) and π-bond delocalized hexagonal structure. These properties are highly beneficial for its extensive use in various significant fields.[29] To integrate graphene into PEM, the electronic and chemical structure of graphene needs to be tuned up. However, doing so is expensive. Graphene oxide (GO) is a derivative of graphene that can be easily and cost effectively synthesized from graphite flakes *via* modified Hummers oxidation method.[30] The surface of GO is covered with various hydrophilic sites including hydroxyl, epoxy and carboxyl, which are highly critical to retain water molecules to facilitate proton conduction even under stringent conditions. The hydrophilic sites present over the GO were reported to have a conductivity of $\sim$0.001 S cm^{-1} at 300 K.[31] However, this value could increase by many folds by substituting the –O–, –OH and –COOH groups with $-SO_3H$ containing organic moieties, due to the rapid ion conducting nature of $-SO_3H$ groups. Furthermore, the interfacial hydrogen bonds (H-bonds) formed between hydrophilic groups of FGO and polymer aid in the construction of extended architecture of proton conducting channels, which further facilitate the diffusion of protons. Several PEMs have been embedded with FGO based fillers. For instance, at 5 wt% of FGO loading, a SPEEK based nanocomposite membrane exhibited 2.02 folds increase in storage modulus and 7.78 folds increase in proton conductivity with respect to corresponding properties of pristine SPEEK membrane. These results were attributed to high mechanical strength of carbon skeletons and good proton conductivity of surface functional groups in FGO.[15] Gahlot *et al.* introduced GO that was functionalized with SO_3H groups into a SPES matrix to prepare composite membrane. They reported that composite membrane with SGO loading from 0.5 to 5 wt% exhibited an increased proton conductivity from 35 to 58 mS cm^{-1}, which is ascribed to increasing the number of SO_3H groups per unit volume of membrane.[32] Shau *et al.* exploited the 4-benzenediazonium sulfonic acid functionalized graphene as filler for the Nafion matrix to prepare high performance nanocomposite membrane for PEFC applications. The uniform dispersion of functionalized graphene in Nafion matrix, attained by strong electrostatic interactions between the polar groups of functionalized graphene and Nafion, increase the water absorption and proton conduction properties of composite membrane.[6] The reports mentioned above indicate that incorporating FGO/functionalized graphene into the polymer matrix enables the membrane to have rich proton conductivity while retaining reasonable mechanical strength. On the other side, the orientation of filler into the polymer matrix also substantially influences the physiochemical, thermomechanical and proton conduction properties of membrane. Exerting magnetic or electrical force is an effective strategy to properly align fillers into the base matrix. Ghalot *et al.* aligned functionalized carbon nanotubes (F-CNTs) within the SPEEK matrix by applying a constant electric field (500 V cm^{-2}). The aligned hybrid membrane exhibited significant improvements in mechanical properties due to high tensile stiffness of vertically aligned F-CNTs when compared to randomly aligned F-CNTs.[33] Beydaghi *et al.* incorporated and subsequently aligned the Fe_3O_4-FGO into the PVA matrix using a constant magnetic field (0.25 T). With aligned Fe_3O_4-FGO, the proton conductivity of composite membrane increases by 1.1 folds, due to the wide and regular proton conduction paths.[34]

Herein, we present unprecedented aligned quadratic hybrid membrane consisting of SPEEK, FPAPB and Fe_3O_4-FGO for the

applications of high temperature and low humidity PEFC. The magnetic characteristics of Fe_3O_4 assist to align the FGO sheets in a direction perpendicular to the cross section of membrane by applying external magnetic field, and hydrophilic characteristics of Fe_3O_4 assist to increase the interfacial compatibility at FGO and polymers interface. The proper orientation of Fe_3O_4-FGO sheets with high interfacial compatibility restructures the aromatic chains of polymers effectively, thereby improves physiochemical thermomechanical and gas barrier properties of the aligned membrane with respect to unaligned membrane.[34] The FGO increases number of SO_3H groups per unit volume of domain in hybrid membrane, which facilitates the transfer of protons through membrane.[6] Besides, the –OH groups on Fe_3O_4 surface generate H-bonds with free water exist in the membrane, which partially slow down the evaporation of water from membrane at high temperature and low humidity conditions and further facilitates the proton transfer through membranes. The effect of alignment of Fe_3O_4-FGO in the blended polymer matrix on morphology, topography, water uptake, dimensional stability, mechanical strength and gas barrier properties of hybrid membranes were intensively investigated. Proton conductivity of aligned quadratic hybrid membranes was also measured at high temperature and low humidity conditions to evaluate the suitability of membranes for conductivity applications.

2. Experimental

2.1. Materials

Iron(II) sulfate heptahydrate ($FeSO_4 \cdot 7H_2O$-99%), iron(III) chloride hexahydrate ($FeCl_3 \cdot 6H_2O$-97%), sodium nitrate ($NaNO_3$-99%) and natural graphite powder (99%) were procured from Alfa Aesar. Potassium permanganate ($KMnO_4$-99.3) was received from Samchun Chemicals, South Korea. Hydrochloric acid (HCl), hydrogen peroxide (H_2O_2-35%), concentrated sulfuric acid, (H_2SO_4-95%) and toluene-99.5% were supplied by Daejung Chemicals, South Korea. *N*,*N*-Dimethylformamide (DMF) was received from Duksan Reagents, South Korea. Bisphenol-A (BPA), decafluorobiphenyl (DFBP), anhydrous potassium carbonate (K_2CO_3), anhydrous *N*,*N*-dimethylacetamide (DMAc-99.8%), anhydrous dimethyl sulfoxide (DMSO-99.8%), anhydrous toluene-99.8%, 3-mercaptopropyl trimethoxy silane (MPTMS-95%) and ammonium hydroxide solution (NH_4OH-5 M) were purchased from Sigma-Aldrich. Poly(ether ether ketone) (PEEK) powder was obtained from Victrex company.

2.2. Functionalization of GO with SO_3H containing organosilane and Fe_3O_4-FGO synthesis

First, the GO was produced according to modified Hummers method using natural graphite powder as the precursor.[30] GO functionalization was then achieved *via* a two-step process: (i) grafting of 3-mercaptopropyl trimethoxy silane (MPTMS) onto the GO surface and (ii) oxidation of mercapto (–SH) group to $–SO_3H$ group using 35% H_2O_2. In a typical method, 250 mg of GO was dispersed in 100 mL of toluene by ultrasonication for 1 h in a round bottom flask. To this admixture, desired volume of MPTMS (1.05 g mL^{-1}) was added drop wise with continuous stirring. The flask was then transferred to a hot plate equipped with a stirrer and spiral water condenser, and reflux reaction was carried out at 110 °C for 24 h. Afterward, the MPTMS-grafted GO was separated *via* high speed centrifugation (12 000 rpm). To remove unreacted impurities, the solid product was washed with a copious amount of DI water, and dried in air at 100 °C for 12 h. The dry MPTMS-grafted GO was further treated with 35% H_2O_2 solution at 25 °C for 24 h to oxidize the –SH to $–SO_3H$. Afterward, the solid was separated *via* centrifugation (12 000 rpm), washed with a copious amount of DI water and then dried in air at 100 °C for 12 h.[21]

The obtained FGO was then anchored with Fe_3O_4 nanoparticles (prepared by co-precipitation method, following a procedure reported in literature[34]) to produce magnetically active solid proton conductors. A 100 mg of FGO was dispersed in 100 mL of DI water by ultrasonication in a beaker. Separately, desired amount of Fe_3O_4 nanoparticles was dispersed in DI water by ultrasonication in a beaker. The Fe_3O_4 suspension was then mixed with FGO suspension, and the resulting mixture was further sonicated for 1 h. Subsequently, the resulting was loaded into a 300 mL Teflon lined stainless steel autoclave and heated at 180 °C for 24 h. Afterward, the solid product was separated using a magnetic bar, washed with a copious amount of DI water and then dried in air at 100 °C for 12 h.

2.3. Synthesis of FPAPB and sulfonation of PEEK

FPAPB was synthesized *via* nucleophilic substitution and polymerization reaction, following a procedure reported in literature.[12] BPA (3.58 g, 15.01 mmol), DFBP (5.77 g, 17.30 mmol), K_2CO_3 (4.84 g, 35.00 mmol), DMAc (25 mL) and toluene (25 mL) were charged together in a dry 100 mL three-necked round bottom flask equipped with a hot plate, magnetic stirrer and Dean–Stark trap apparatus with N_2 gas inlet. Initially, the mixture was refluxed at 160 °C (oil bath) for 6 h to carry out polymerization reaction. Next, the reaction temperature was elevated to 180 °C and was maintained for 24 h to eliminate water produced due to toluene distillation. After completing the reaction, the obtained pale yellow viscous solution was precipitated into solvent of methanol/acetone/deionized water (8 : 1 : 1, v/v/v). The resultant precipitate was repeatedly washed, filtered and then dried in air at 100 °C for 12 h.

PEEK was sulfonated *via* electrophilic substitution reaction, following a procedure reported in literature.[35–37] A 28 g of dry PEEK powder was first dissolved in 300 mL of con. H_2SO_4 by mechanical stirring (300 rpm speed) at 40 °C. After dissolution, the solution temperature was increased to 60 °C, and stirring continued for desired time at the same temperature. Then, the obtained viscous solution was gradually precipitated into copious amount of ice-cold water and repeatedly washed until attain a neutral pH. Sulfonated polymer was dried (100 °C for 12 h) and kept for further use. The DS of the polymer varied according to the acid concentration and volume, and reaction time and temperature.

2.4. Preparation of hybrid membrane

Blend of SPEEK (90%) and FPAPB (10%) was first prepared by dissolving two individual polymers together in 10 mL of DMF

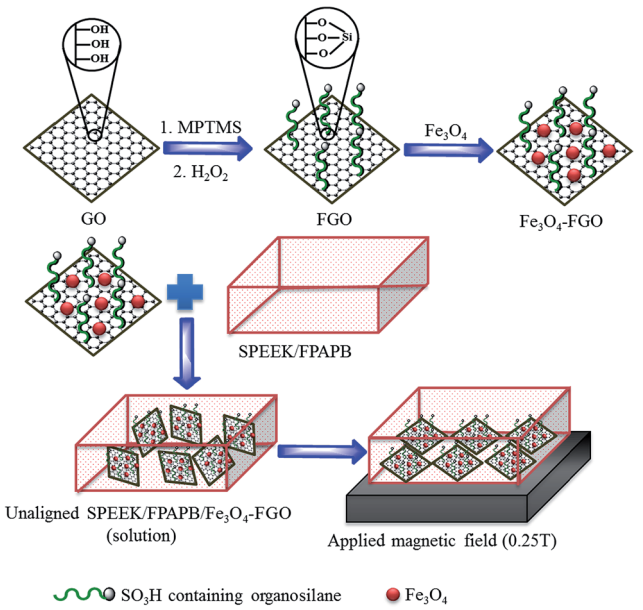

Scheme 1 Preparation process of aligned quadratic hybrid membrane.

(10 wt%) by magnetic stirring (at 60 °C for 48 h). Then, the desired amount of Fe_3O_4-FGO with the weight ratio of 1, 3, 5 or 7 wt% was impregnated into above blend solution, and the mixture was ultrasonicated until attain a homogeneous dispersion of Fe_3O_4-FGO. The mixture was casted on a clean glass plate placed over the flat magnet (able to generate 0.25 T), and dried at 80 °C for 12 h. The aligned hybrid membrane thus formed were peeled off and further dried at 120 °C for 2 h to remove solvent residues. Fe_3O_4-FGO (without magnetic field) and GO based membranes were also fabricated to systematically compare the properties of unaligned Fe_3O_4-FGO and GO membranes with respect to aligned membrane. The fabricated membranes such as SPEEK, SPEEK/FPAPB, SPEEK/FPAPB/GO-*X* and SPEEK/FPAPB/Fe_3O_4-FGO-*X* have been designated as SP, SPF, SPFG-*X* and SPFSGF-*X*, respectively, where, *X* represents the wt% of GO or Fe_3O_4-FGO in the hybrid membrane. The thicknesses of dry hybrid membranes were measured at three random points, and are in the range from 70 to 90 μm. Scheme 1 illustrates the fabrication process of aligned quadratic hybrid membrane.

2.5. Pre-treatment of membrane

All the prepared membrane specimens were pre-treated before the proton conductivity measurement as follows. The specimens were first immersed in 1 M H_2SO_4 for 1 h at 90 °C to activate the acidic functional groups and were brought to hydrate with DI water for 24 h at room temperature to increase the water content in membrane.[14]

3. Instrument and apparatus details

Routine procedures given below were followed to characterize the prepared specimens. Surface morphologies of the GO, FGO and Fe_3O_4-FGO were characterized by field emission scanning electron microscope (FE-SEM) (SUPRA 40VP) equipped with quantitative energy dispersive X-ray (EDX) spectrometer. Surface as well as cross-sectional morphologies of the hybrid membranes were also characterized by FE-SEM. Imaging of all specimens was carried out after sputtering with elemental osmium. Surface topographies of the membranes were scrutinized by using atomic force microscopy (AFM) (multimode-8 model). Imaging was performed in contact mode under a cantilever frequency of 300 kHz, and an ultra-sharp antimony doped silicon tip with a radius of 20 nm and spring constant of 40 N m^{-1} was used throughout the study. Line profiles of the membrane surface were also measured to obtain information about height variation at particular section of the membrane surface. The deviation of actual membrane surface topography [$Z(x,y)$] from an ideal atomically smooth surface (μ) is known as surface roughness. Root mean square (RMS) roughness (S_q) may afford useful information about the topography of membrane surface, and it can be calculated using the following equation, as described in the literature.[6]

$$S_q = \sqrt{\frac{1}{MN}\sum_{K\to 0}^{M-1}\sum_{l\to 0}^{N-1}[Z(x_k - y_l) - \mu]} \quad (1)$$

where M and N are the respective x and y points in the specimen, $Z(x,y)$ is the surface and

$$\mu = \frac{1}{MN}\sum_{K\to 0}^{M-1}\sum_{l\to 0}^{N-1} Z(x_k - y_l) \text{ is the mean height} \quad (2)$$

The chemical structures of FPAPB and SPEEK were studied by using Fourier transform nuclear magnetic resonance (FT-NMR) spectrometer (JNM-ECA-600 MHz), with anhydrous DMSO-d_6 as solvent. Fourier transform infrared (FT-IR) spectrometer (Perkin Elmer) was used to investigate the intermolecular stretching in prepared membranes. The spectra were recorded over the frequency range 4000–400 cm^{-1}, and KBr pellet method was used for sample preparation. The M_n, M_w and PDI index of FPAPB were estimated by gel permeation chromatography (GPC) (HLC-8320GPC-Tosoh Corporation) equipped with RI detector and calibrated with polystyrene. High resolution X-ray diffractometer (HR-XRD) (X′ pert-MRD) was used to investigate the crystalline faces of specimens of GO, FGO, Fe_3O_4-FGO. The spectra were recorded using CuKα radiation over the scattering 2-theta angle 5–90°. Thermogravimetric analyser (TGA) (Q50-TA Instruments) was used to measure the thermal stability of prepared samples. Measurement was conducted from 30 to 800 °C at a heating rate of 5 °C min^{-1} under N_2 atmosphere. Thermal behaviours of membranes were further scrutinized using differential scanning calorimetry (DSC) (Q20-TA instruments) at a heating rate of 10 °C min^{-1} under N_2 atmosphere. Dynamic mechanical analyzer (DMA) (Q800-TA instruments with a tan delta sensitivity of 0.0001) was used to measure the temperature dependent mechanical stabilities of fabricated membranes. The weights of membrane specimens were measured using a Denver four digit counter balance (model: S-234). The length and width of membrane specimens were measured using an ABSOLUTE

digital Vernier caliber (Mitutoyo-model: 500-196-20). The thicknesses of membrane specimens were measured by an ABSOLUTE digimatic indicator (Mitutoyo-model: ID-S112X).

4. Measurements

4.1. Water uptake

Water uptake measurements were carried out to measure the water retention capabilities of membranes.[17] Prior dried (at 100 °C for 5 h) membrane specimens were weighed and submerged in DI water at various temperatures (20, 40, 60 and 80 °C) for 24 h to attain equilibrium. Afterward, the water on the surface of specimens was carefully blotted with tissue paper and weighed again. Each reported value is the average of three measurements with the error level of +1.0. The water uptake was calculated using the equation given below:

$$\text{Water uptake } (\%) = \left[\frac{W_{\text{wet}} - W_{\text{dry}}}{W_{\text{dry}}}\right] 100$$

where W_{dry} and W_{wet} are the respective weights (g) of specimens before and after water uptake.

4.2. Volume change

Dimensional stabilities of the membrane specimens were evaluated from volume change after water uptake at various temperatures (20, 40, 60 and 80 °C) for 24 h. Each reported value is the average of three measurements with the error level of +1.0. The volume change was calculated using the equation given below:

$$\text{Volume change } (\%) = \left[\frac{V_{\text{wet}} - V_{\text{dry}}}{V_{\text{dry}}}\right] 100$$

where V_{dry} and V_{wet} are the respective volumes (cm^3) of specimens before and after water uptake.

4.3. Ion exchange capacity

Acid–base back titration was carried out to determine the ion exchange capacity (IEC) of membrane specimens. The detailed procedure of IEC measurement can be found in the literature.[38] Each reported value is the constant of two consecutive titrations with the error limit of +0.05. The IEC was calculated using the following equation:

$$\text{IEC } (\text{meq. g}^{-1}) = \frac{\text{volume of NaOH consumed} \times \text{concentration of NaOH}}{\text{weight of dry specimen}}$$

4.4. Hydration number

Hydration number (λ) indicates the number of water molecules absorbed per unit volume of SO_3H groups in the membranes.[33] This was calculated from the water uptake and IEC of membranes using the equation given below:

$$\lambda = \left[\frac{\text{water uptake}}{18.01}\right]\left[\frac{10}{\text{IEC}}\right]$$

where 18.01 is the molecular weight of water in g mol^{-1}.

4.5. Oxidative stability

Oxidative stability of the membrane specimens was determined as follows. The specimens were dried in air at 100 °C for 5 h, and the weights of dry specimens were measured. The dry specimens were then submerged into the Fenton's reagent (3% H_2O_2 + 2 ppm $FeSO_4$) in a hermetic flask at 80 °C. The stabilities of the specimens were evaluated from rupture time and remaining weights.[39]

4.6. Proton conductivity

The proton conductivity of membrane specimens (30 mm × 5 mm) was measured in the longitudinal direction using alternative current impedance spectroscopy (Sci-tech instrument, Keithley-2400 source meter and four electrode Bekk-tech cell conjugated with gas flow option). The detailed procedure of proton conductivity measurement can be found in the literature.[21] The longitudinal conductivity (σ) of specimens as a function of temperature under low humidity was calculated using the equation given below:

$$\sigma\ (\text{mS cm}^{-1}) = \frac{L}{RTW}$$

where L is the distance between four Pt electrodes in cm (0.42 cm), R is the ionic resistance of specimen in ohms, and T and W are the thickness and width of specimen in cm. Each specimen was subjected to several repeated measurements to ensure the reproducibility.

4.7. Electrical conductivity

The electrical conductivity of SPF, SPFSGF-5 (unaligned) and SPFSGF-5 (aligned) membrane specimens was measured using Keithley Electrometer coupled with four Pt electrodes. A piece of dry specimen (30 mm × 5 mm) was placed across the Pt electrodes and current was measured as a function of applied voltage, as described in the literature.[33] The following equation was used to calculate the electrical conductivity (σ) of membrane specimens.

$$\sigma\ (\Omega^{-1}\ \text{cm}^{-1}) = \frac{G \times l}{A}$$

where G is the conductance of specimen in Siemens, l is the thickness of specimen in cm and A is the active surface of specimen in cm^2.

4.8. Gas permeability

Gas permeability of the membrane specimens was measured under fully anhydrous condition using constant volume/variable pressure method, as described in the literature.[40] The gas was supplied at a flow pressure rate of 1 barrer, and the temperature was kept constant at 30 °C throughout the measurement. Each reported value is the average of three measurements and the error limit for gas permeability is +0.05. All variables used for permeability calculation are identified as follows: the gas diffusivity coefficient is D ($cm^2\ S^{-1}$), the solubility coefficient is S [cm^3 (cm^2 scm Hg)$^{-1}$], the constant permeation volume is V_p, the feed pressure is P_f (cm Hg), the time of pressure change from P_{p1} to P_{p2}

is Δt (mins), the specimen length is L (cm), the active area is A (cm^2) and the operating temperature is T (kelvin). The gas permeability of membranes specimens was calculated using the equation given below:

$$\text{Permeability (barrer)} = DS = V_p L(P_{p2} - P_{p1})/ [ART\Delta t(P_f - (P_{p2} + P_{p1})/2)]$$

5. Results and discussion

5.1. Morphological properties

Fig. 1 depicts FE-SEM micrographs of GO, FGO and Fe_3O_4-FGO. The FGO exhibits a crumpled structure (Fig. 1b), similar to the morphology of pristine GO (Fig. 1a), indicating that GO microstructure was not deformed significantly after grafting SO_3H containing organosilane. Such crumpled structure of FGO is highly beneficial to anchor the nanoparticles throughout their active surface. The Fe_3O_4-FGO micrograph (Fig. 1c) shows that Fe_3O_4 nanoparticles ranging from 15 to 30 nm are randomly loaded throughout the surface of FGO. This observation confirms that hydrothermal is an effective method to load size controlled Fe_3O_4 on the surface of FGO. The peaks found at about 2.3 keV (due to S), and at about 0.7 and 6.3 keV (due to Fe) in the EDX spectrum (Fig. 1e) confirms the presence of SO_3H and Fe_3O_4 in the Fe_3O_4-FGO. To verify the density as well as distribution of SO_3H and Fe_3O_4 on the surface of Fe_3O_4-FGO, quantitative energy dispersive elemental mapping were captured, and the images are presented in Fig. S1.† The SO_3H (Fig. S1d†) and Fe_3O_4 (Fig. S1f†) are distributed throughout the surface of Fe_3O_4-FGO rather being located at particular site, which help to improve the proton conductivity and magnetic properties of Fe_3O_4-FGO.

The essential macroscopic properties, including water uptake, mechanical strength, proton conductivity and gas barrier properties, are greatly influenced by internal morphology and filler dispersion of the hybrid membranes.[14] Cross-sectional FE-SEM images of pristine SP, SPFSGF-5 (unaligned) and SPFSGF-5 (aligned) membranes are displayed in Fig. 2a–c, respectively. The SP membrane exhibits a thin cross-section with many internal defects (Fig. 2a), caused due to the incompatibility between interconnected SO_3H channels and hydrophobic polymer backbones. It is clear from Fig. 2b and c that the internal morphology of SP membrane becomes rougher after incorporation of Fe_3O_4-FGO, which is due to the crumpled structure of Fe_3O_4-FGO. Besides, the internal defects are observed to be partially cured in hybrid membranes that should be ascribed to the blending of high viscous FPAPB. Meanwhile, the dispersion of Fe_3O_4-FGO is uniform and denser in the membrane matrix for the aligned case, whereas not uniform for the unaligned case. The uniform dispersion of filler in aligned membrane is a result of strong interfacial interactions (H-bonding and π–π interactions) between polymers and Fe_3O_4-FGO achieved by proper orientations of Fe_3O_4-FGO. In such a way, co-continuous proton conducting channels are generated through the aligned membrane, which enable the proton conduction faster. The top-view FE-SEM images of pristine SP and SPF membranes were captured to determine the essential changes in the membrane surface after reinforcing with FPAPB, and are shown in Fig. 2d and e, respectively. The pristine SP membrane exhibits the surface of pores and pinholes (marked in Fig. 2d insert), caused due to the incompatibility between SO_3H groups and hydrophobic polymer backbones, consistent with the corresponding cross section. After blending with high viscous FPAPB, the pinholes over the surface of membrane were dramatically reduced (Fig. 2e), indicating that FPAPB

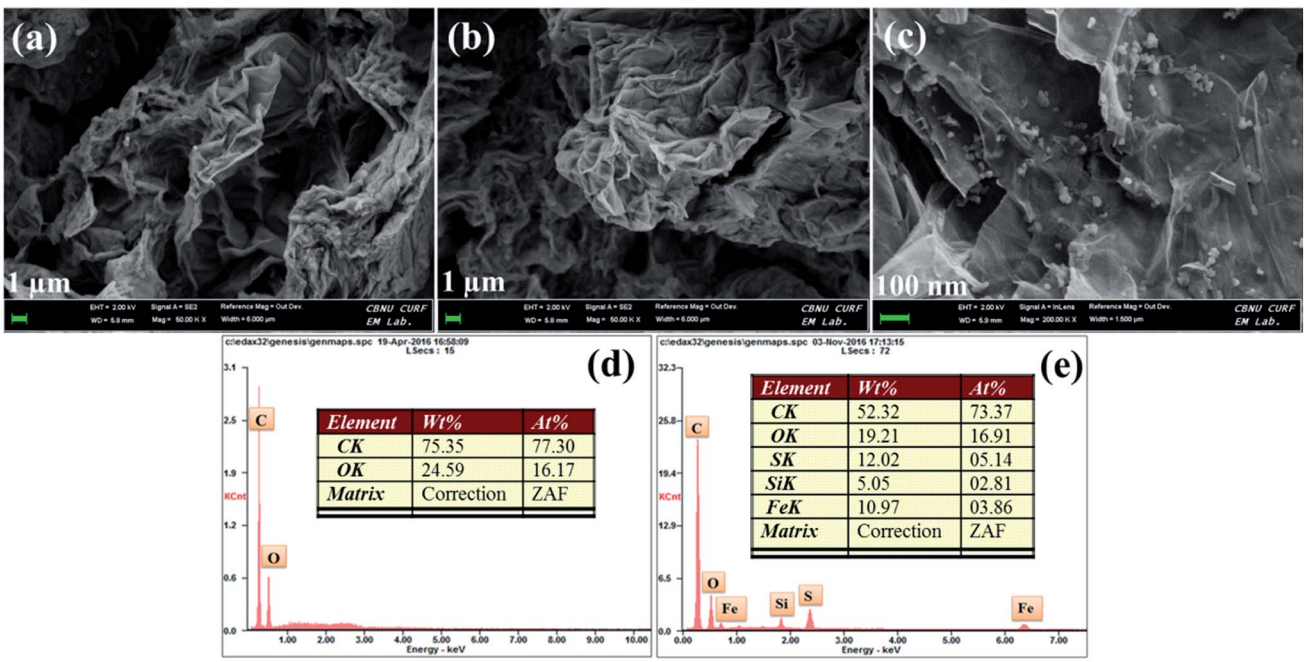

Fig. 1 FE-SEM images of (a) GO, (b) FGO and (c) Fe_3O_4-FGO; corresponding EDX spectra of (d) GO and (e) Fe_3O_4-FGO.

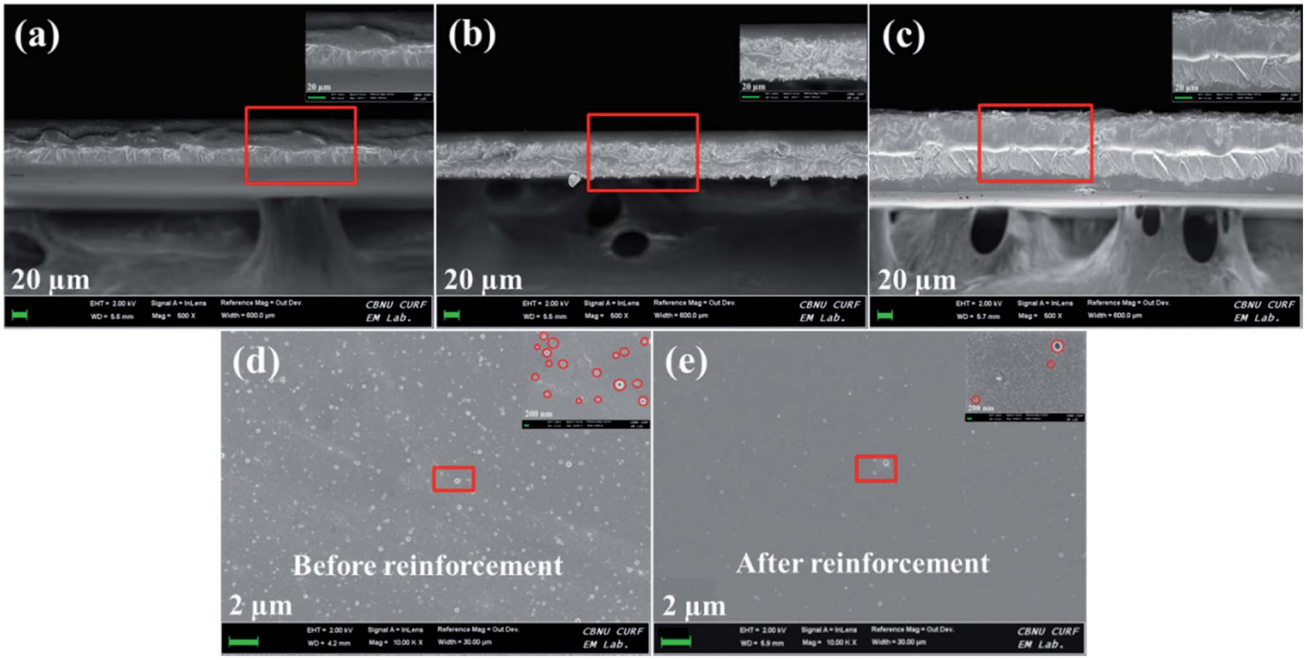

Fig. 2 Cross sectional FE-SEM images of membranes of (a) SP, (b) SPFSGF-5 (unaligned) and (c) SPFSGF-5 (aligned); top view FE-SEM images of membranes of (d) SP and (e) SPF.

reinforcement enables the formation of membrane with low surface defects. However, pores are still retained in the SPF membrane, which are beneficial for selective permeation of protons rather than gas molecules. This reinforcement phenomenon is further beneficial to improve oxidative stability, mechanical strength and thermal stability of SPF membrane. Scheme 2 illustrates the possible interactions exerted between individual components in quadratic hybrid membrane. Fig. 3 shows the AFM topographies and line profiles of hybrid membranes. SPF membrane exhibits the surface with limited

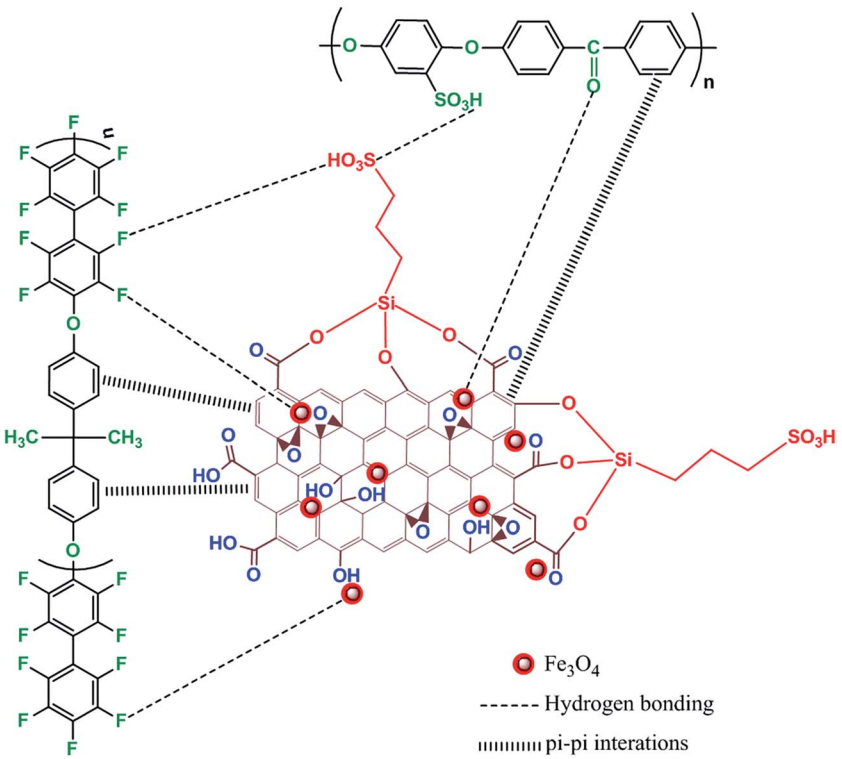

Scheme 2 Possible interactions exerted between individual components in quadratic hybrid membrane.

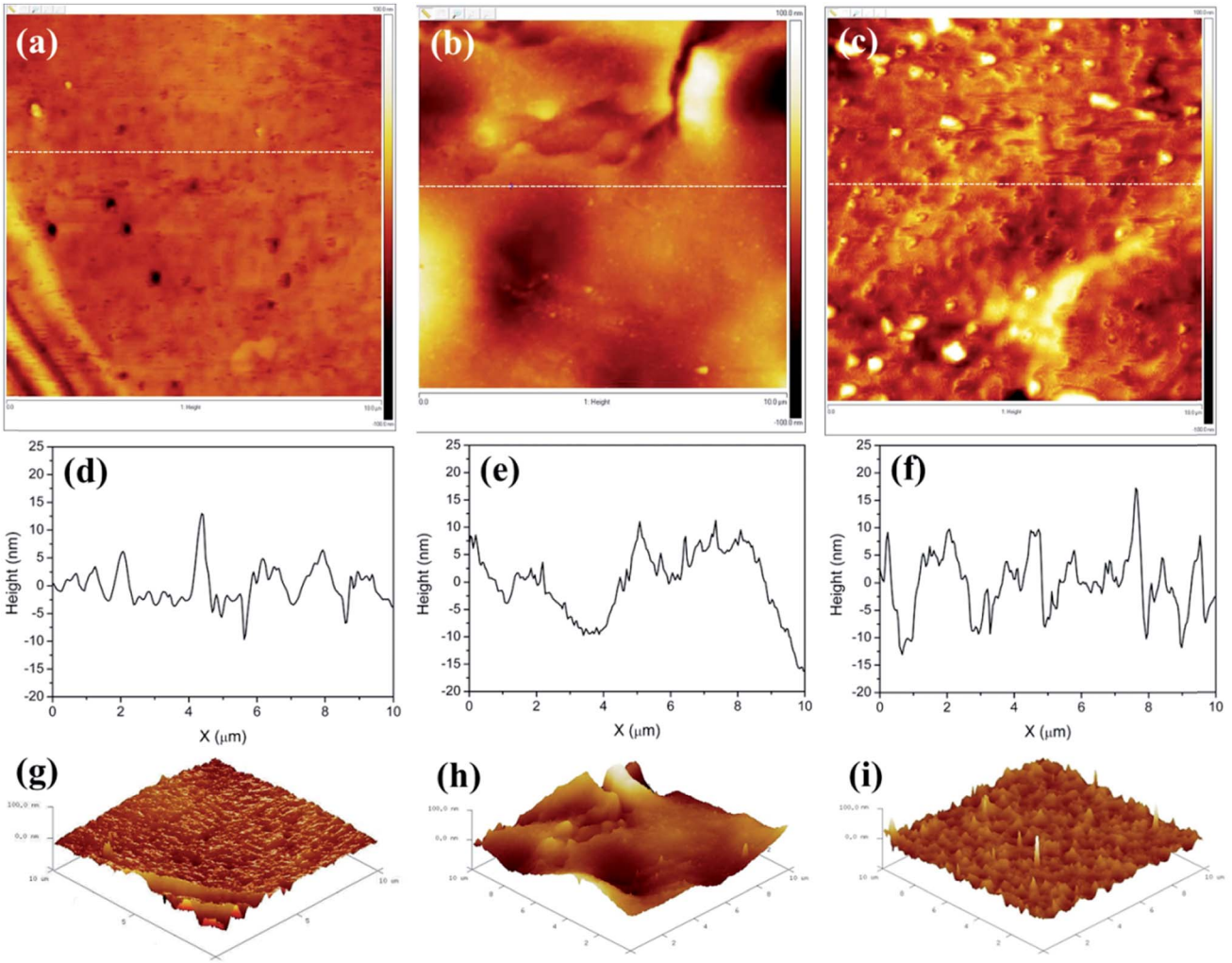

Fig. 3 2D AFM topographies of membranes of (a) SPF, (b) SPFSGF (unaligned) and (c) SPFSGF (aligned); corresponding line profiles of membranes of (d) SPF, (e) SPFSGF (unaligned) and (f) SPFSGF (aligned); 3D AFM topographies of membranes of (g) SPF, (h) SPFSGF (unaligned) and (i) SPFSGF (aligned).

pinholes (Fig. 3a), which is consistent with corresponding top-view FE-SEM image. After incorporating and aligning Fe_3O_4-FGO, the membranes exhibit entirely different surface behaviour with respect to SPF membrane. In the case of SPFSGF-5 (unaligned) (Fig. 3b), the big subsidences and protrusions are randomly distributed in membrane surface, while the small spikes and hidden are uniformly and densely distributed in membrane surface of the SPFSGF-5 (aligned) case (Fig. 3c), which is due to the parallel alignment of Fe_3O_4-FGO to the surface of membrane. The RMS roughness of above mentioned membranes was calculated using the eqn (1). Compared to SPF (3 nm), the SPFSGF-5 (unaligned) and SPFSGF-5 (aligned) membranes exhibited higher RMS roughness of 25 and 15 nm respectively, which may attributed to the crumbled structure of Fe_3O_4-FGO.[38]

5.2. Structural properties

The chemical structures of FPAPB and SPEEK were investigated by means of NMR spectra; details, including figures and explanation, are given in ESI.†[12,41] The number average molecular weight (M_n), weight average molecular weight (M_w), mean average molecular weight (M_Z) and poly disperse index (PDI) of the synthesized FPAPB were evaluated by GPC. The detailed explanation is given in ESI.†[42]

FT-IR spectra of pristine SP, SPF and SPFSGF-5 membranes are provided in Fig. 4. The absorption bands at 3422 cm^{-1} in pristine SP and 3476 cm^{-1} in both SPF and SPFSGF-5 indicate the presence of –OH group (related to hydrogen bonds) in membranes. The absorption bands at 3067 cm^{-1} in pristine SP and 3056 in both SPF and SPFSGF-5 indicate the presence of –OH group (related to the acidic groups) in membranes. The characteristic bands found at 1220, 1078 and 1012 cm^{-1} are common for all three membranes, which are assigned to symmetric and asymmetric stretching modes of O=S=O in SO_3H groups of SPEEK.[40,43,44] Compared to SP, the hybrid membranes reveal a new low intensity peak at 2784 cm^{-1}, which is attributed to C–F stretching of aromatic rings in FPAPB. The slight peak shifts (especially –OH peaks) in SPF and SPFSGF-5

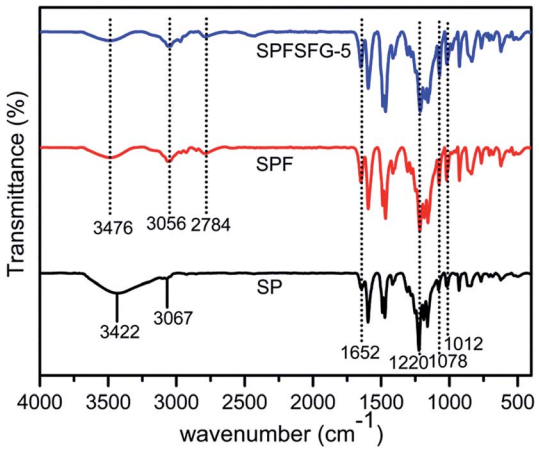

Fig. 4 FT-IR spectra of membrane of SP, SPF and SPFSGF-5.

membranes can also be observed with respect to pristine SP membrane, which are due to strong H-bonding interactions exerted between the polar groups (–SO_3H, –O–, C═O, –OH, –CO_2H, –F) of SPEEK, FPAPB and Fe_3O_4-FGO.

The crystalline faces of GO, FGO and Fe_3O_4-FGO were analysed by using XRD, and the corresponding patterns are presented in Fig. S3.† The successful oxidation of graphite to GO is ensured by diffraction peak found at 10.9° with an inter-planer spacing of 7.5 A, which is ascribed to 001 reflection plane of GO.[45] After grafting SO_3H containing organosilane on the surface of GO, the diffraction peak shifted to higher 2θ (24.4°) with an inter-planer spacing of 3.1 A. The reduction in inter-planar spacing is due to partial restacking of GO layers *via* π–π interactions, caused by the removal of oxygen functional groups after functionalization. In Fe_3O_4-FGO case, the Fe_3O_4 revealed the reflection planes of (111), (220), (311), (400), (422), (511), (440), (620) and (533) at 2θ of 24.1°, 33.2°, 35.6°, 41.0°, 54.0°, 57.3°, 62.4°, 71.8° and 75.7°, respectively,[46] whereas the FGO exhibited a broad peak at 2θ of 24.4°. This observation confirms that the Fe_3O_4 (face cantered cubic structure) were successfully loaded over the surface of FGO.

5.3. Thermal behaviours

TGA thermographs of GO, FGO and Fe_3O_4-FGO are displayed in Fig. S4.† GO and FGO show different stages of degradation as follows: (i) below 100 °C, due to the elimination of physisorbed free water molecules, (ii) 100–150 °C, due to the pyrolysis of bound water molecules, (iii) 150–270 °C, owing to the decay of surface functional groups and (iv) above 600 °C, attributed to the destruction of carbon skeletons. By comparison, the FGO exhibits slightly higher weight loss during the third stage (*i.e.* 21.63% for GO and 27.3% for FGO), due to the existence of excess SO_3H groups on the FGO. The thermal stability of FGO is significantly improved after loading the Fe_3O_4 nanoparticles, as evidenced by higher residual weight of Fe_3O_4-FGO *i.e.* 78.16% at 800 °C. TGA thermographs of fabricated membranes are displayed in Fig. 5a. All the membranes exhibit similar sort of three step weight drops: (i) 30–230 °C, attributed to the evaporation of free and bound water molecules present in the membrane, (ii) 290–400 °C, owing to the decay of SO_3H groups in the polymer chains and (iii) 450–800 °C, related to the decomposition of aromatic chains of polymers. Compared to pristine SP, the hybrid membranes exhibited retarded manner of weight drops. Therefore, addition of FPAPB and Fe_3O_4-FGO is justified, as they effectively improve the thermal stability of SP by preventing the relaxation of aromatic polymer chains through interfacial interactions. At 800 °C, the remaining weights of pristine SP, SPF, SPFG-5, SPFSGF-5 (unaligned) and SPFSGF-5 (aligned) membranes are 37.06%, 47.95%, 42.76%, 43.80% and 46.17%, respectively. Higher remaining weight of hybrid membranes than pristine SP is attributed to FPAPB polymer because its C–F bonds have high resistivity against the free radicals (generated during thermal decomposition). Overall, the thermal stabilities of fabricated hybrid membranes are more than sufficient to tolerate the operating temperatures of high temperature PEFC.

DSC thermograms of the prepared membranes are shown in Fig. 5b. Pristine SP membrane exhibits the glass transition temperature (T_g) at 213 °C, which is lower than that of PEEK (340 °C).[14] This low T_g is due to the presence of more SO_3H groups in SPEEK chains, which considerably reduce the crystallinity of polymer. While the SPF membrane shows T_g at 185 °C, indicating that FPAPB blending further reduce the crystallinity of SP membrane, due to its amorphous nature. Apart from crystallinity, the rigidity significantly influences the T_g of membranes, as reported in literature.[27] The incorporation of Fe_3O_4-FGO reduced the T_g of SPF membrane to 180 °C, due to the strong interfacial interactions between polar groups

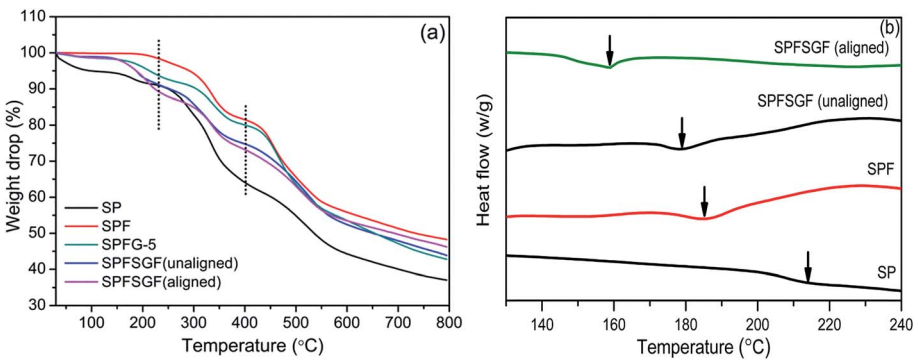

Fig. 5 (a) TGA and (b) DSC curves of pristine SP and hybrid membranes.

(–SO_3H, –O–, C═O, –F) of polymers and functional groups of Fe_3O_4-FGO. These interactions slow down the reorganization of aromatic chains of SPEEK and FPAPB, thereby increase the rigidity of membranes. A further reduction in T_g is noticed for the aligned membrane, indicating that the reorganization of polymer chains is further slowed down while aligning the Fe_3O_4-FGO perpendicularly to the cross-section of membrane.

5.4. Temperature dependent mechanical stability and oxidative stability

Since, adequate mechanical stabilities of the PEMs are crucial for long-term operation of PEFCs. DMA was performed to investigate the temperature dependent mechanical stabilities of as prepared membranes, and the obtained results are displayed in Fig. 6. The SP, SPFSFG-5 (unaligned) and SPFG-5 (aligned) membranes were selected as representatives. The SP membrane exhibited the maximum storage modulus of 1463 MPa, while it increased by 1.24 folds for the SPFSFG-5 (unaligned) membrane (1819). High mechanical strength of C–F bonds in FPAPB and high Young's modulus of carbon skeletons in Fe_3O_4-FGO collectively offer a high storage modulus to the hybrid membrane. Furthermore, the mutual π–π interaction between unsaturated C–C bonds in carbon skeletons of Fe_3O_4-FGO and benzene rings of FPAPB and SPEEK strictly restrict the movements of polymer chains, which further improve the mechanical strength of hybrid membrane. Meanwhile, the unprecedented storage modulus is noticed for aligned membrane (*i.e.* 2582 MPa) when compared to unaligned membrane. This is attributed to the perpendicular alignment of Fe_3O_4-FGO to the cross-section of membrane, which toughens the membrane upto a reasonable margin. The tan δ value of aligned membrane is increased by 1.05 folds compared to unaligned membranes and by 1.07 folds compared to SP membrane (Fig. 6b).

Oxidative stability is a paramount factor to PEM and it is need to be high to attain extended durability of PEM during fuel cell operation.[47–49] *In situ* and *ex situ* durability tests can measure the oxidative stability of PEM and Fenton's test is an indication of *ex situ* durability.[22] Fig. 7d depicts the remaining weights and rupture times of as prepared membranes when immersed in Fenton's solution at 80 °C. It can be seen that the pristine SP membrane is ruptured after 4 h of time and exhibits 92.7% of remaining weight, due to the higher number of pinholes in membrane, as shown in FE-SEM image. However, the hybrid membranes are stable upto 12 h of time, and the remaining weights of SPF, SPFG-5 SPFSGF-5 (aligned) and SPFSGF-5 (unaligned) membranes are 97.2, 93.5, 91.2 and 89.1%, respectively. It is noteworthy to mention that high radical resistivity of C–F bonds in FPAPB is responsible for long time stability of hybrid membrane, which can bring long-term durability of membrane during PEFC operation.

5.5. Water uptake, volume change, IEC, hydration number and bound water content

Water uptake, volume change, IEC, hydration number and bound water content are the crucial parameters to determine the proton conductivity of PEM.[33] Table S1† and Fig. 7a depicts the temperature (20, 40, 60 and 80 °C) dependent water uptakes of as prepared membranes. At 80 °C, the pristine SP membrane is observed to be soluble (due to its high water swollen behaviour), while the SPF membrane shows 33.41% water uptake. This demonstrates that FPAPB blending prevent the swelling of SP membrane by precluding the excess trapping of water. In the case of SPFG-5, SPFSGF-5 (unaligned) and SPFSGF-5 (aligned) membranes, the observed maximum water uptakes are 54.61, 59.13 and 62.15%, respectively, at 80 °C. With incorporation of GO or Fe_3O_4-FGO, the water uptake of SPF membrane increased, due to the more hydrophilicity of GO and Fe_3O_4-FGO. Meanwhile, the maximum water uptake of aligned membrane is observed to be little higher compared to that of unaligned membrane. The only possible reason for that is proper orientation of Fe_3O_4-FGO in the polymer matrix, which generates excess number of voids at polymer–filler interface to hold water. The temperature dependent water uptakes of SPFSGF-*X* (aligned) membranes increase as increase filler content, but the water uptakes decrease above 5 wt%, owing to the aggregation of fillers (Fig. 7a). Table S1,† Fig. 7b show the volume changes occurred in membranes after water uptake at different temperatures (20, 40, 60 and 80 °C). The volume change of hybrid membranes demonstrates a similar dependence to that of water uptake. Compared to SPF, the SPFG-5, SPFSGF-5 (unaligned) and SPFSGF-5 (aligned) membranes exhibited higher % of maximum volume changes *i.e.* 32.31, 38.20 and 40.42%, respectively, at 80 °C. This should be attributed to the

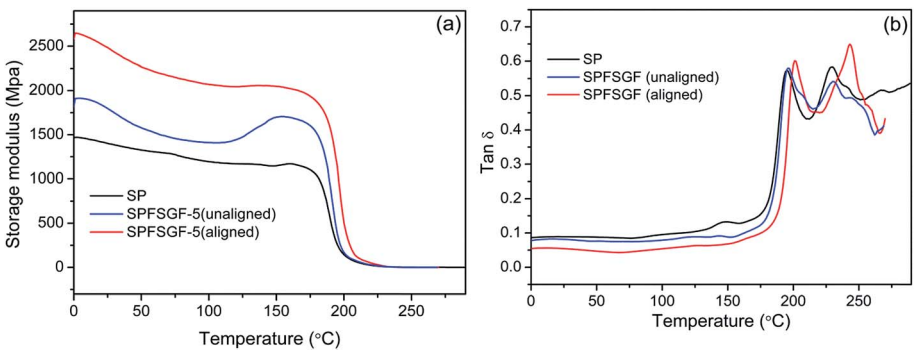

Fig. 6 DMA curves of (a) storage modulus and (b) tan δ of pristine SP and hybrid membranes.

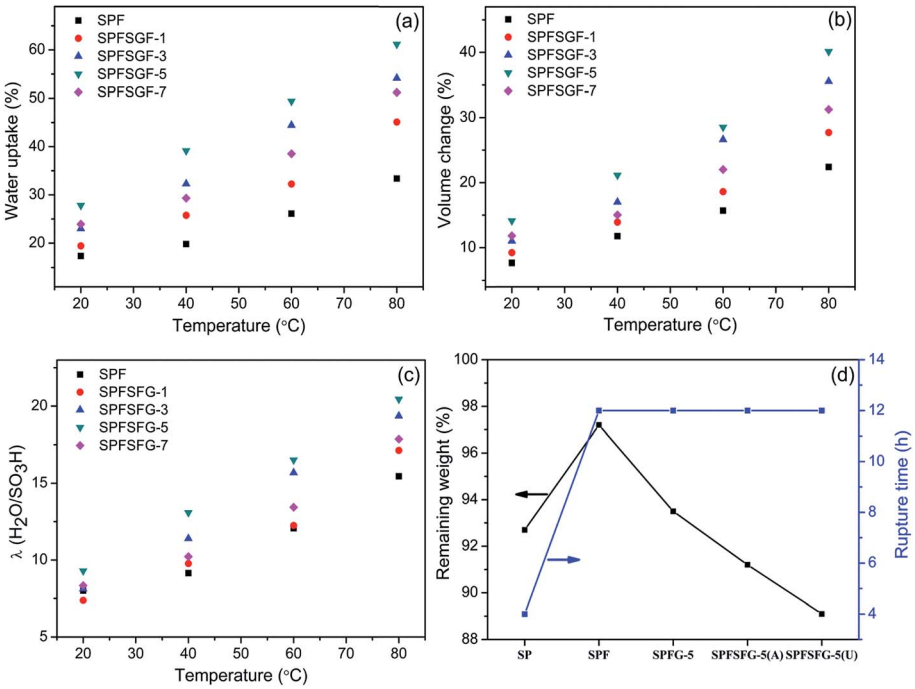

Fig. 7 (a) Water uptake, (b) volume change (c) hydration number and (d) oxidative stability (at 80 °C) of hybrid membranes.

higher water uptake characteristics of corresponding membranes. The increased volume change of SPFSGF-*X* (aligned) membranes upon increasing filler content is ascribed to higher water uptake, caused by more hydrophilicity of Fe_3O_4-FGO (Fig. 7b). IEC is directly proportional to density of ionic sites in the PEM.[47] Table 1 lists the IEC values of as prepared membranes. IEC for SPF membrane was 1.20 meq. g^{-1}, which is lower than the IEC of pristine SP membrane (1.60 meq. g^{-1}), indicating that blending of FPAPB significantly reduced the per unit volume of ionic sites in the membrane. However, the IEC values of SPFG-5, SPFSGF-5 (unaligned) and SPFSGF-5 (aligned) membranes are observed to be higher compared to SPF membrane. It is noteworthy to mention that the existence of adequate ionic sites on the surface of GO and Fe_3O_4-FGO subsequently increases the per cluster volume of ionic sites in SPF matrix, which increases the IEC of hybrid membranes. Number of water molecules absorbed per unit volume of SO_3H groups in the membrane is known as hydration number (λ). Table S1† and Fig. 7c reveal the λ values of as prepared membranes at different temperatures (20, 40, 60 and 80 °C). The λ value exhibited by pristine SP membrane is 7.58 at 20 °C, it considerably increased to 15.45 when temperature rose to 60 °C. Compared to SP (soluble at 80 °C), the SPF, SPFG-5, SPFSFG-5 (unaligned) and SPFSGF-5 (aligned) membranes exhibited the λ values of 15.45, 19.55, 19.76 and 20.77, respectively, at 80 °C. Enhanced λ value of the hybrid membranes is associated with the higher water uptakes, which bring more possibility for vehicle type proton conduction in the hybrid membranes. In general, two types of water are available in the PEM: (i) covalently bound hydrophilic functionalities named as bound water and (ii) non-covalently bound hydrophilic moieties named as free water.[33] Bound water is mostly contributed to proton conductivity of PEM rather than free water. The % of bound water content in prepared membranes was calculated from TGA

Table 1 IEC, hydration number (λ), water uptake, proton conductivity (σ) under 100% RH, activation energy (E_a) and gas permeability of membranes

Specimens	IEC (meq. g^{-1}) (±0.05)	λ (H_2O/SO_3H) (±0.1)	Water uptake (%) (±1.0)	σ (mS cm^{-1}) (±0.1)		E_a (kJ mol^{-1}) (±0.5)	Permeability (barrer)	
				20 °C	100 °C		H_2	O_2
SP	1.60	—	—	20.61	—	—	11.35	0.72
SPF	1.20	15.45	33.41	7.33	41.03	19.62	8.76	0.39
SPFG-5	1.55	19.55	54.61	11.33	59.96	—	7.23	0.31
SPFSGF-5 (unaligned)	1.66	19.76	59.13	24.79	72.75	15.13	5.86	0.28
SPFSGF-1 (aligned)	1.46	17.13	45.13	13.41	55.23	17.63	—	—
SPFSGF-3 (aligned)	1.57	19.36	54.19	19.10	66.78	16.72	—	—
SPFSGF-5 (aligned)	1.66	20.77	62.15	26.61	75.16	14.31	4.51	0.23
SPFSGF-7 (aligned)	1.59	17.87	51.25	14.93	58.73	15.97	—	—

curves (100–230 °C), and the values are shown in Table 2. The SPFSGF-5 (unaligned) and SPFSGF-5 (aligned) membranes have highest amount of bound water compared to the other membranes, which are 8.65 and 9.32%, respectively.

5.6. Proton conductivity and Arrhenius plot

Proton conductivity is a key factor to PEM and it is necessary to be high to attain improved operational voltage and current output in PEFC.[40] The water uptake and IEC of hybrid membranes are found to be increased upto a reasonable margin when integrating and further aligning the high surface Fe_3O_4-FGO in SPF matrix, which consequently increase the proton conductivity of membrane. The proton conductivity of hybrid membranes is increased by three possible factors of additives: (i) excess concentration of ion conducting SO_3H provided by high surface FGO, (ii) intrinsic character of Fe_3O_4 nanoparticles to retain bound water molecules both physically and chemically and (iii) creation of high compact pores by perpendicularly aligned Fe_3O_4-FGO at polymer–filler interface, which perform as free voids to absorb excess water. Since the migration of H_3O^+, $H_5O_2^+$ and $H_9O_4^+$ ions are encouraged by water retention channels, the proton conductivity of membranes increased as the same manner of water uptake and IEC.

The proton conductivities of membranes were measured at various temperatures under 100% and 20% RH. Table S2† and Fig. 8a display all obtained proton conductivities of membranes under 100% RH. Peak proton conductivities of the SP, SPFG-5, SPFSGF-5 (unaligned) and SPFSGF-5 (aligned) membranes (representatives) are found to be 47.59, 59.96, 72.75 and 75.16 mS cm^{-1}, respectively. High proton conductivity of SPFSGF-5 membrane is ascribed to Fe_3O_4-FGO, which increases the per unit volume of SO_3H groups in membrane, thereby generating the additional ion conducting channels to contact protons. Furthermore, the proper orientation of integrated Fe_3O_4-FGO assist to form wide ion conducting channels in aligned membrane, which further enhance the conductivity compared to unaligned membrane. Proton conductivities of SPFSGF-*X* (aligned) membranes are found to be increased by 2.8–5.8 folds upon increasing the temperature from 20 to 100 °C (Fig. 8a), which may due to the rapid proton mobility with temperature.

A reasonable proton conductivity of PEM at high temperature under low humidity is significant to develop cost competitive and efficient PEFC system. However, most of the reported PEMs suffered by conductivity decline at high temperature under low humidity, due to the evaporation of water. Table S2† and Fig. 8c demonstrates all obtained proton conductivities of membranes under 20% RH. Peak proton conductivities of the SP, SPFG-5, SPFSGF-5 (unaligned) and SPFSGF-5 (aligned) membranes (representatives) are found to be 7.68, 7.33, 10.06 and 11.13 mS cm^{-1}, respectively. Lower conductivity of SP membrane is owing to the membrane dehydration, caused by inadequate volume of bound water molecules, as shown in Table 2. SPFSGF-*X* (aligned) membranes afforded the peak proton conductivities of are in the range between 5.67 and 11.13, which is a few folds higher than that of Nafion-112 membrane, inferring that the prepared hybrid membranes can be applicable for high temperature and low humidity PEFC. Table S3† summarized various GO based membrane properties reported in literatures, for comparison with present study.[6,15,21,22,40,50–57]

Activation energy (E_a) is required for proton travel through PEM and lower activation energy enables the fast proton travel in PEM. Besides, E_a is an essential factor to determine the proton conduction mechanism that occurred in membrane. E_a values of membranes were calculated from the slope of Arrhenius plots, which are derived from conductivity values using the following Arrhenius equation:[50]

$$\ln \sigma = \ln \sigma_0 - E_a/RT$$

where σ is the proton conductivity (mS cm^{-1}), σ_0 is the pre-exponential factor (mS cm^{-1}), E_a is the activation energy required for proton travel (kJ mol^{-1}), R is the gas constant (J mol^{-1} K^{-1}) and T is the temperature (kelvin). As shown in Tables 1 and 2, a relatively lower E_a is noticed for the SPFSGF-*X* compared to SPF membrane, due to the distribution of excess density of SO_3H and other conducting groups throughout the SPFSGF-*X* membrane, caused by the dispersion of Fe_3O_4-FGO. Considering that the E_a for Grotthuss mechanism is in the range of 9.65–38.59 kJ mol^{-1} and for vehicle mechanism is only about 16.4 kJ mol^{-1}.[58,59] The obtained results indicate that both Grotthuss and vehicle mechanisms coexist in membranes under 100% RH, while Grotthuss mechanism dominates more under 20% RH, due to the lack of free water molecules. Overall, the incorporation of

Table 2 Free and bound water contents, proton conductivity (σ) under 20% RH, activation energy (E_a), electronic conductivity ($\sigma_{(E)}$) of membranes

Specimens	Free water (%) (±0.2)	Bound water (%) (±0.2)	σ (mS cm^{-1}) (+0.1) 20 °C	σ (mS cm^{-1}) (+0.1) 120 °C	E_a (kJ mol^{-1}) (±0.5)	$\sigma_{(E)}$ (mS cm^{-1})
SP	5.04	3.99	2.18	7.68	—	0.025
SPF	0.74	1.41	0.23	3.10	31.19	—
SPFG-5	1.13	4.86	2.69	7.33	—	—
SPFSGF-5 (unaligned)	1.41	8.65	3.76	10.06	22.41	0.20
SPFSGF-1 (aligned)	—	—	1.17	5.67	27.20	—
SPFSGF-3 (aligned)	—	—	2.51	8.38	25.84	—
SPFSGF-5 (aligned)	1.88	9.32	3.66	11.13	21.31	0.27
SPFSGF-7 (aligned)	—	—	1.81	6.20	23.99	—

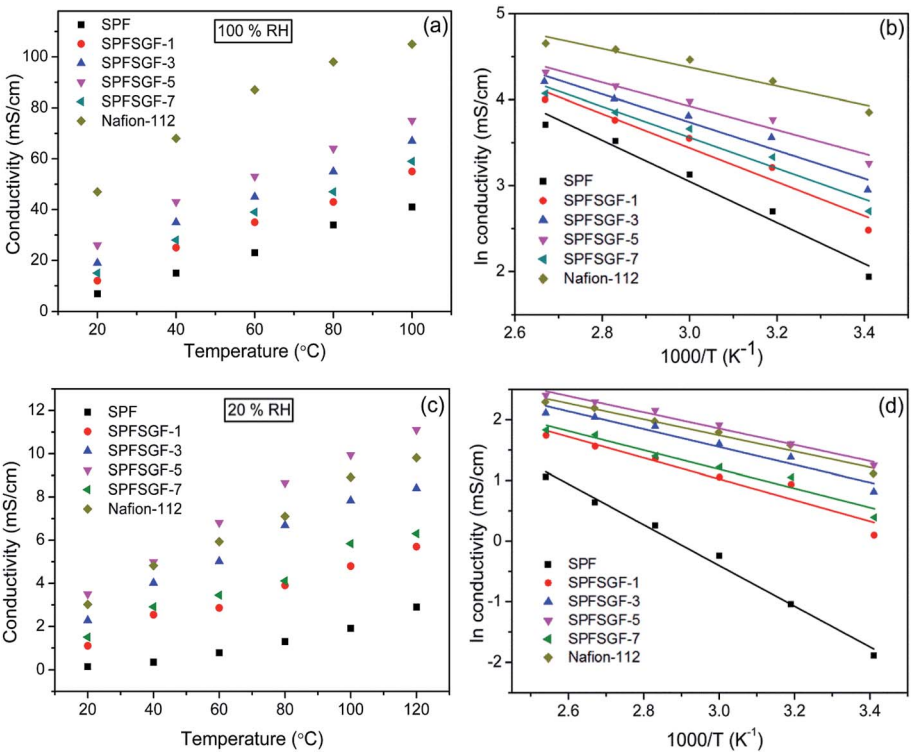

Fig. 8 Temperature variant proton conductivities of aligned hybrid membranes (a) under 100% RH and (c) under 20% RH; corresponding Arrhenius plots for proton conductivities (b) under 100% RH and (d) under 20% RH.

aligned Fe_3O_4-FGO into SPF matrix results a low activation energy barrier pathway within the membrane, which affords enhanced proton conductivity under fully hydrated as well as low humidity condition.

5.7. Current–voltage characteristics

Fig. 9 shows the current–voltage (*i*–*v*) characteristics of pristine SP, SPFSGF-5 (unaligned) and SPFSGF-5 (aligned) membranes. There is a dramatic change observed in *i*–*v* characteristics of the hybrid membranes as compared to the SP membrane. SP membrane exhibits almost negligible current at all applied voltages, whereas current of the hybrid membrane increase as increase the voltage from 0–10 V, due to the existence of electrically conducting additive *i.e.* Fe_3O_4-FGO. Furthermore, the current of the hybrid membrane is further enhanced upon aligning the Fe_3O_4-FGO perpendicularly to the cross section of membrane. As shown in Table 2, the calculated electrical conductivity of the SPFSGF-5 (aligned) membrane (0.27 mS cm^{-1}) is 1.35 folds higher than that of unaligned membrane (0.20 mS cm^{-1}) and 10.8 folds higher than that of pristine SP membrane (0.025 mS cm^{-1}), which is due to high percolation threshold of aligned Fe_3O_4-FGO. However, the obtained electrical conductivities of hybrid membranes are very low *i.e.* lower than the level which affect the open circuit voltage (OCV) of membrane during PEFC operation.[33]

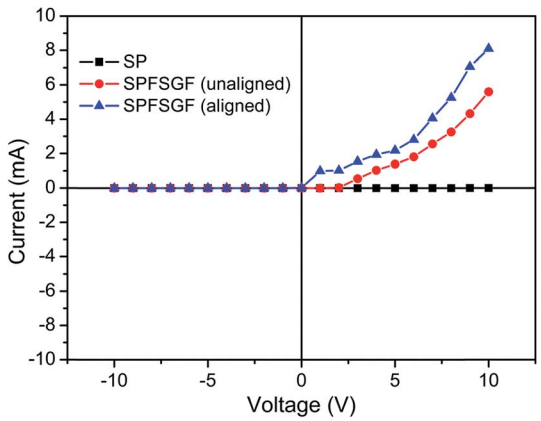

Fig. 9 Current–voltage (*i*–*v*) characteristics of the pristine SP and hybrid membranes.

5.8. Gas permeability

Considering the problems of H_2 crossover from the anode to the cathode through PEM (causes irregular fuel usage and generation of water without any useful work) as well as O_2 crossover from cathode to anode through PEM (causes mixed potential of oxidant with fuel and reduction in cell voltage), the gas permeability measurements were conducted for the prepared membranes. Fig. 10 shows the obtained gas permeability values of as prepared membranes. H_2 permeability of the pristine SP membrane is 11.35 barrer, it is 1.22 folds higher than that of Nafion-117 membrane (9.30 barrer),[40] due to the higher number of pinholes in membrane, as shown in FE-SEM image. By comparison, a 1.29 folds lower H_2 permeability was observed for the SPF membrane (8.76 barrer), indicating that blending of

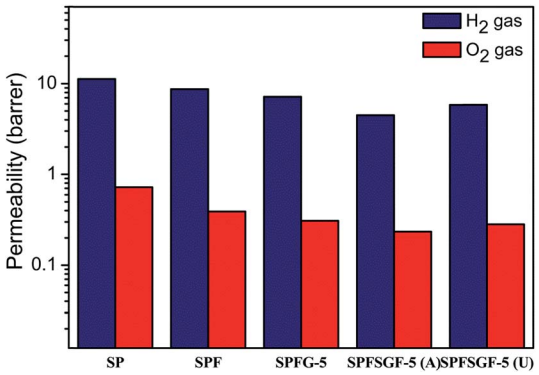

Fig. 10 H_2 and O_2 permeability of pristine SP and hybrid membranes.

FPAPB significantly reduced the number of pinholes in SP membrane. In the case of SPFSGF-5 (aligned) membrane, the perpendicularly aligned Fe_3O_4-FGO is tightly wrapped with polymer chains *via* H-bonding and π–π interactions, which generate aligned supramolecular structures across the cross-section of membrane. These supramolecular structures generate a strong barrier effect against the permeation of gas molecules through the membrane. Therefore, the SPFSGF-5 (aligned) membrane shows a very lower H_2 permeability (4.51 barrer) compared to SPF membrane. Nevertheless, the SPFSGF-5 (unaligned) membrane shows H_2 permeability of 5.86 barrer, which is still 1.29 folds higher than that of aligned membrane. On the other side, all membranes exhibit a similar behaviour of O_2 permeability as in the H_2 permeability. The O_2 permeability of SP, SPF, SPFG-5, SPFSGF-5 (aligned) and SPFSGF-5 (unaligned) membranes are 0.72, 0.39, 0.31, 0.23 and 0.28 barrer, respectively.

6. Conclusion

Efficient, but cost-competitive, aligned quadratic hybrid membranes were successfully fabricated using facile solution casting approach by applying a constant magnetic field. The quadratic hybrid membranes with magnetically aligned Fe_3O_4-FGO show better performance compared to membranes with randomly aligned Fe_3O_4-FGO. Furthermore, among the aligned membranes, the SPFSGF-5 exhibits better performance. While the water uptake, IEC, proton conductivity and gas barrier properties of the membrane are improved greatly, the membrane still retained reasonable mechanical strength. Blending of FPAPB and incorporation of aligned Fe_3O_4-FGO reinforces the SPEEK chains *via* hydrogen bonding and π–π interaction, which strengthen the membrane mechanically and thermally by 1.7 and 1.2 folds, respectively. Prepared membranes exhibit considerable proton conductivity at high temperature under low humidity, and have reduced activation energy for proton conduction due to incorporation of aligned Fe_3O_4-FGO. The reasonable improvements in physiochemical, thermomechanical and proton conduction properties of quadratic hybrid indicate that addition of FPAPB and Fe_3O_4-FGO with SPEEK significantly affects the performance of PEM in a better way. The comprehensive affairs and good stabilities make the aligned quadratic hybrid membranes as a promising candidate for high temperature and low humidity PEFC.

Conflict of interest

The all authors declare that they have no conflict of interest.

Acknowledgements

This work was supported by the Korea Institute of Energy Technology Evaluation and Planning (KETEP) and the Ministry of Trade, Industry & Energy (MOTIE) of the Republic of Korea (No. 20164030201070). This research was supported by Basic Science Research Program through the National Research Foundation of Korea (NRF) funded by the Ministry of Science, ICT and future Planning (NRF-2017R1A2B4005230).

References

1 B. C. Steele and A. Heinzel, *Nature*, 2001, **414**, 345–352.
2 P. P. Edwards, V. L. Kuznetsov, W. I. F. David and N. P. Brandon, *Energy Policy*, 2008, **36**, 4356–4362.
3 B. Bae, K. Miyatake and M. Watanabe, *ACS Appl. Mater. Interfaces*, 2009, **1**, 1279–1286.
4 L. Carrette, K. A. Friedrich and U. Stimming, *ChemPhysChem*, 2000, **1**, 162–193.
5 C. Y. Wang, *Chem. Rev.*, 2004, **104**, 4727–4765.
6 A. K. Sahu, K. Ketpang, S. Shanmugam, O. Kwon, S. Lee and H. Kim, *J. Phys. Chem. C*, 2016, **120**, 15855–15866.
7 M. A. Barique, L. Wu, N. Takimoto, K. Kidena and A. Ohira, *J. Phys. Chem. B*, 2009, **113**, 15921–15927.
8 B. P. Tripathi and V. K. Shahi, *ACS Appl. Mater. Interfaces*, 2009, **1**, 1002–1012.
9 K. Yoshimura and K. Iwasaki, *Macromolecules*, 2009, **42**, 9302–9306.
10 S. Takamuku and P. Jannasch, *Macromolecules*, 2012, **45**, 6538–6546.
11 T. Miyahara, T. Hayano, S. Matsuno, M. Watanabe and K. Miyatake, *ACS Appl. Mater. Interfaces*, 2012, **4**, 2881–2884.
12 A. R. Kim, M. Vinothkannan and D. J. Yoo, *Int. J. Hydrogen Energy*, 2017, **42**, 4349–4365.
13 Z. Q. Jiang, X. S. Zhao and A. Manthiram, *Int. J. Hydrogen Energy*, 2013, **38**, 5875–5884.
14 M. Vinothkannan, A. R. Kim, K. S. Nahm and D. J. Yoo, *RSC Adv.*, 2016, **6**, 108851–108863.
15 Y. Heo, H. Im and J. Kim, *J. Membr. Sci.*, 2013, **425**, 11–22.
16 A. M. Baker, L. Wang, W. B. Johnson, A. K. Prasad and S. G. Advani, *J. Phys. Chem. C*, 2014, **118**, 26796–26802.
17 A. Bagheri, M. Javanbakht, H. Beydaghi, P. Salarizadeh, A. Shabanikia and H. S. Amoli, *RSC Adv.*, 2016, **6**, 39500–39510.
18 R. P. Pandey, A. K. Das and V. K. Shahi, *ACS Appl. Mater. Interfaces*, 2015, **7**, 28524–28533.
19 G. G. Kumar, J. Shin, Y. C. Nho, I. S. Hwang, G. Fei, A. R. Kim and K. S. Nahm, *J. Membr. Sci.*, 2010, **350**, 92–100.

20 A. K. Mohanty, E. A. Mistri, S. Banerjee, H. Komber and B. Voit, *Ind. Eng. Chem. Res.*, 2013, **52**, 2772–2783.
21 H. Zarrin, D. Higgins, Y. Jun, Z. W. Chen and M. Fowler, *J. Phys. Chem. C*, 2011, **115**, 20774–20781.
22 N. Zhang, B. Wang, Y. Zhang, F. Bu, Y. Cui, X. Li, C. Zhao and H. Na, *Chem. Commun.*, 2014, **50**, 15381–15384.
23 V. Tricoli and F. Nannetti, *Electrochim. Acta*, 2003, **48**, 2625–2633.
24 P. Kalappa and J. H. Lee, *Polym. Int.*, 2007, **56**, 371–375.
25 Q. H. Yang, J. Liu, J. Yang, M. P. Kapoor, S. Inagaki and C. Li, *J. Catal.*, 2004, **228**, 265–272.
26 Z. Y. Li, X. J. Yue, G. W. He, Z. Li, Y. H. Yin, M. Y. Gang, H. Wu and Z. Y. Jiang, *Int. J. Hydrogen Energy*, 2015, **40**, 8398–8406.
27 Z. G. Shao, P. Joghee and I. M. Hsing, *J. Membr. Sci.*, 2004, **229**, 43–51.
28 A. K. Geim, *Science*, 2009, **324**, 1530–1534.
29 M. V. Kannan and G. Gnana Kumar, *Biosens. Bioelectron.*, 2016, **77**, 1208–1220.
30 W. S. Hummers and R. E. Offeman, *J. Am. Chem. Soc.*, 1958, **80**, 1339.
31 M. R. Karim, K. Hatakeyama, T. Matsui, H. Takehira, T. Taniguchi, M. Koinuma, Y. Matsumoto, T. Akutagawa, T. Nakamura, S. Noro, T. Yamada, H. Kitagawa and S. Hayami, *J. Am. Chem. Soc.*, 2013, **135**, 8097–8100.
32 S. Gahlot, P. P. Sharma, V. Kulshrestha and P. K. Jha, *ACS Appl. Mater. Interfaces*, 2014, **6**, 5595–5601.
33 S. Gahlot and V. Kulshrestha, *ACS Appl. Mater. Interfaces*, 2015, **7**, 264–272.
34 H. Beydaghi and M. Javanbakht, *Ind. Eng. Chem. Res.*, 2015, **54**, 7028–7037.
35 P. Xing, G. P. Robertson, M. D. Guiver, S. D. Mikhailenko, K. Wang and S. Kaliaguine, *J. Membr. Sci.*, 2004, **229**, 95–106.
36 S. M. J. Zaidi, S. D. Mikhailenko, G. P. Robertson, M. D. Guiver and S. Kaliaguine, *J. Membr. Sci.*, 2000, **173**, 17–34.
37 R. K. Nagarale, G. S. Gohil and V. K. Shahi, *J. Membr. Sci.*, 2006, **280**, 389–396.
38 V. Parthiban, S. Akula, S. G. Peera, N. Islam and A. K. Sahu, *Energy Fuels*, 2016, **30**, 725–734.
39 M. Vinothkannan, R. Kannan, A. R. Kim, G. G. Kumar, K. S. Nahm and D. J. Yoo, *Colloid Polym. Sci.*, 2016, **294**, 1197–1207.
40 L. Zhao, Y. Li, H. Zhang, W. Wu, J. Liu and J. Wang, *J. Power Sources*, 2015, **286**, 445–457.
41 R. Naresh Muthu, S. Rajashabala and R. Kannan, *Int. J. Hydrogen Energy*, 2015, **40**, 1836–1845.
42 D. J. Yoo, S. H. Hyun, A. R. Kim, G. G. Kumar and K. S. Nahm, *Polym. Int.*, 2011, **60**, 85–92.
43 W. Dai, Y. Shen, Z. Li, L. Yu, J. Xi and X. Qiu, *J. Mater. Chem. A*, 2014, **2**, 12423.
44 A. Rahnavard, S. Rowshanzamir, M. J. Parnian and G. R. Amirkhanlou, *Energy*, 2015, **82**, 746–757.
45 Z. Bo, X. Shuai, S. Mao, H. Yang, J. Qian, J. Chen, J. Yan and K. Cen, *Nature*, 2014, **4**, 1–8.
46 Y. Wang, B. Li, Y. Zhou and D. Jia, *Nanoscale Res. Lett.*, 2009, **4**, 1041–1046.
47 H.-R. Jang, E.-S. Yoo, R. Kannan, J.-S. Kim, K. Lee and D. J. Yoo, *Colloid Polym. Sci.*, 2017, **295**, 1059–1069.
48 K. H. Lee, J. Y. Chu, A. R. Kim, K. S. Nahm, C. J. Kim and D. J. Yoo, *J. Membr. Sci.*, 2013, **434**, 35–43.
49 B. Kim, R. Kannan, K. S. Nahm and D. J. Yoo, *J. Dispersion Sci. Technol.*, 2016, **37**, 1315–1323.
50 Z. Q. Jiang, X. S. Zhao, Y. Z. Fu and A. Manthiram, *J. Mater. Chem.*, 2012, **22**, 24862–24869.
51 H. C. Chien, L. D. Tsai, C. P. Huang, C. Y. Kang, J. N. Lin and F. C. Chang, *Int. J. Hydrogen Energy*, 2013, **38**, 13792–13801.
52 H. Beydaghi, M. Javanbakht and E. Kowsari, *Ind. Eng. Chem. Res.*, 2014, **53**, 16621–16632.
53 R. P. Pandey, A. K. Thakur and V. K. Shahi, *ACS Appl. Mater. Interfaces*, 2014, **6**, 16993–17002.
54 T. Ko, K. Kim, M.-Y. Lim, S. Y. Nam, T.-H. Kim, S.-K. Kim and J.-C. Lee, *J. Mater. Chem. A*, 2015, **3**, 20595–20606.
55 H. Beydaghi, M. Javanbakht, A. Bagheri, P. Salarizadeh, H. G. Zahmatkesh, S. Kashefi and E. Kowsari, *RSC Adv.*, 2015, **5**, 74054–74064.
56 Y. H. Liu, J. T. Wang, H. Q. Zhang, C. M. Ma, J. D. Liu, S. K. Cao and X. Zhang, *J. Power Sources*, 2014, **269**, 898–911.
57 A. K. Mishra, N. H. Kim, D. Jung and J. H. Lee, *J. Membr. Sci.*, 2014, **458**, 128–135.
58 Y. Jin, S. Z. Qiao, J. C. D. da Costa, B. J. Wood, B. P. Ladewig and G. Q. Lu, *Adv. Funct. Mater.*, 2007, **17**, 3304–3311.
59 K. D. Kreuer, *Chem. Mater.*, 1996, **8**, 610–641.